Jefferson Lab

System and Infrastructure Design Review
May 7-9, 2008

Hall D Trigger Simulation

The GLUEX Collaboration
E. Chudakov, D. Doughty, and A. Somov

April 29, 2008

Contents

1 Introduction

The goal of the experiment is the search for hybrid/exotic mesons produced by a photon beam on a liquid hydrogen target. These mesons would decay to final states containing charged pions and photons. The charged particles are detected by the drift chambers. They give signals in one of the calorimeters and may hit the forward TOF scintillators. The charged particle momentum will not be evaluated in the first-level trigger. The photons are detected with the calorimeters and their energy will be evaluated at this stage.

The first-level trigger can use signals from:

- the forward calorimeter (FCAL);
- the barrel calorimeter (BCAL);
- the forward time-of-flight plastic scintillator detector (TOF);
- the plastic scintillator start-counter;
- the photon beam tagger plastic scintillator counter.

Final states of the hybrid meson decays are not expected to differ strongly from the ordinary photoproduction processes, which could have provided a signature for their separation from the background on the trigger level. Therefore, the experiment needs a soft trigger which accepts nearly all hadronic events produced by the beam photons in a certain energy range. At this stage, only the events outside of the required energy range are considered background.

Purely electromagnetic interactions of the beam in the target, as such pair production, although strongly suppressed in the spectrometer by the solenoidal magnetic field and the detector arrangement, can give signals in the individual detectors. They can either fire the trigger, or pile up in low energy hadronic events, thus faking larger energies and increasing the background rate.

2 Photon Beam and Photoproduction Rate

Photons are produced by the 12-GeV electron beam on a diamond crystal via both incoherent and coherent Bremsstrahlung processes. The spectrum of the coherent photons is concentrated in several peaks of different strengths, whose positions as well as the degree of the photon's linear polarization depends on the crystal's orientation. The coherent component is relatively stronger at smaller Bremsstrahlung angles. The beam parameters have been optimized for GLUEX [1]:

- The diamond crystal is 20 μm thick;
- The collimator of a 3.4 mm diameter is positioned at a 76 m distance from the crystal;
- The main coherent Bremsstrahlung peak is located at $\sim 8.4 - 9.0$ GeV;

The experiment should be able to run with the photon flux of 100 MHz in the main peak $E \sim 8.4 - 9.0$ GeV. This intensity can be provided by a ~ 2 μA electron beam. At the initial stage, the experiment will run at a beam intensity ten times lower.

An ideal trigger would select only the events in the range of 8.4-9.0 GeV.

The calculated beam spectra above the photoproduction threshold are shown in Fig. 1(a). In this range of 0.15-12 GeV, the tagger rate is 10 GHz. Because of the collimation, the beam rate is about 7 times lower at 1.5 GHz. In the useful range of 8.4-9.0 GeV the tagger rate of 250 MHz is 2.5 times higher than the beam rate.

The tagger could provide an efficient way to select the energy range of the accepted events. However, at the high beam intensity the tagger rate is too high, since about 50% of accelerator pulses arriving at 500 MHz will provide at least one hit in the useful range of the tagger.

The hadronic photoproduction rate on a 30 cm long liquid hydrogen target was calculated using the full photoproduction cross section, tabulated by the PDG group [2] (see Fig. 1(b)).

The expected rates are summarized in Table 1. The full photoproduction rate of 360 kHz is dominated by the low energy part. The rate in the coherent peak is 16 kHz.

Should the first-level trigger select only events for beam energies above 2 GeV, it would reduce the trigger rate to 100 kHz.

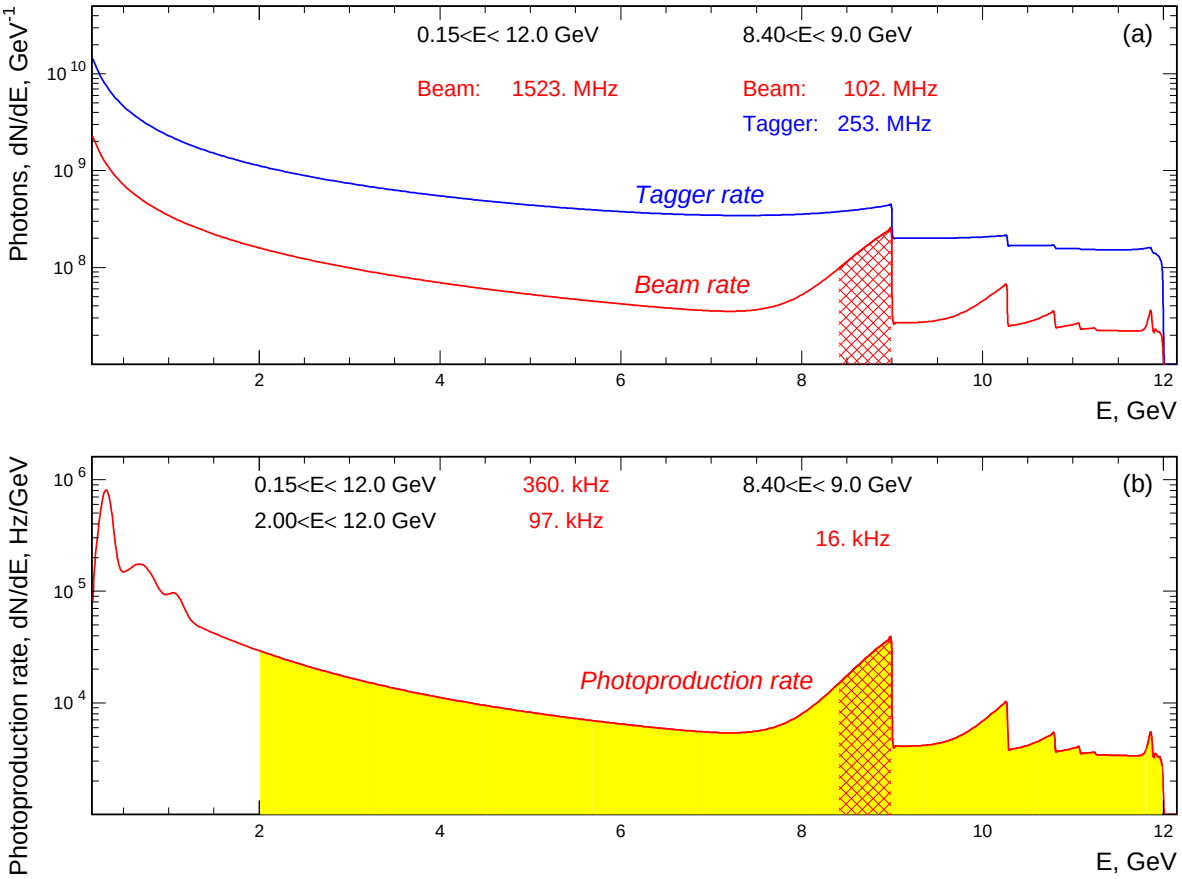

Figure 1: The top figure (a) shows the energy spectra for the photons before and after the collimator. The former spectrum (in blue) demonstrates the expected rate on the beam tagger, while the latter one (in red) is the spectrum of the beam seen by the experiment. The collimated beam has the coherent peak enhanced relatively to the incoherent contribution. The useful beam energy area of 8.4-9.0 GeV is shaded. The bottom figure (b) shows the hadronic photoproduction rate. The useful area is shaded. A broader shaded area, of 2.0-12. GeV indicates the energy range which can likely be identified by the first-level trigger.

Rates	Energy range, GeV		
	0.15 - 12.	2.0 - 12.	8.4 - 9.0
Tagger	10 GHz	4.0 GHz	250 MHz
Beam	1.5 GHz	670 MHz	100 MHz
Photoproduction	360 kHz	100 kHz	16 kHz

Table 1: The expected rates at the high luminosity running, in various energy intervals. The bottom row shows the hadronic rate.

3 Simulation of Photoproduction

The photoproduction processes have been simulated using the following scheme:

- The energy spectrum of the interacting photons was calculated using the beam energy spectrum and the total photoproduction cross section (see Fig. 1(b));
- At the beam energies below 3 GeV an admixture of several dominant reactions was simulated, their relative differential cross sections were taken from the existing data;
- Above 3 GeV the PYTHIA generator [3] was used, slightly adapted for low energies.

PYTHIA was designed and tuned by the authors for much higher energies. Special efforts were taken by the HERMES collaboration to adapt it to the HERA electron energy of ∼30 GeV. We slightly adapted the version from HERMES to the energies as low as 3 GeV, and compared the PYTHIA results with some experimental data. At 9 GeV PYTHIA underestimates the total photoproduction cross section, providing $\sim$ 80 μb instead of $\sim$ 120 μb. However, the partial cross sections from PYTHIA, scaled up by a factor 120/80=1.5 are in a reasonable agreement with the data (see Table 2).

process		Experiment		PYTHIA	
$\gamma p \to$	via	E_γ, GeV	σ, μb	E_γ, GeV	σ, μb
1 prong		9.3	8.5±1.0	9.0	6.2
3 prong		9.3	64.4±1.5	9.0	59.0
5 prong		9.3	34.2±0.9	9.0	44.0
7 prong		9.3	6.8±0.3	9.0	8.3
$p\pi^+\pi^-$		9.3	14.7±0.6	9.0	14.5
	$p\rho^\circ$	9.3	13.5±0.5	9.0	13.0
$p\pi^+\pi^-\pi^\circ$		9.3	7.5±0.8	9.0	7.0
	$p\omega$	9.3	1.9±0.3	9.0	1.4
$p2\pi^+2\pi^-$		9.3	4.1±0.2	9.0	3.7

Table 2: Comparison of the partial cross sections provided by PYTHIA with the data. The PYTHIA results were scaled by a factor of 1.5.

At the energies below 1 GeV the dominant process is the single pion production, which is not simulated well by PYTHIA. On the other hand, these processes have been well parametrized in the framework of MAID and SAID systems [4]. At energies below 3 GeV only about 10 processes with small multiplicities comprise more than 95% of the total cross section. The differential cross sections for these processes have been well measured. Above 3 GeV more reactions with higher multiplicities and more complex differential cross sections step in. Therefore, we applied the hybrid approach, using

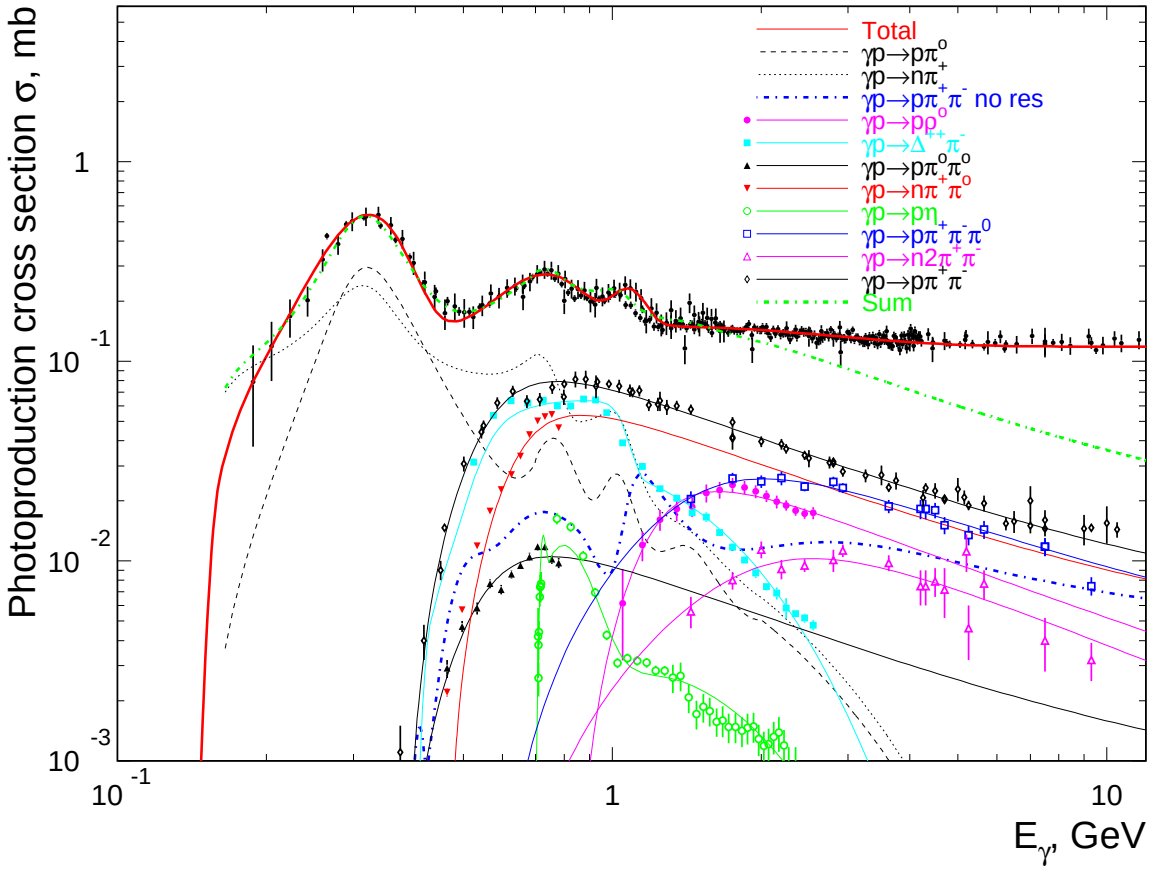

Figure 2: The total photoproduction cross section (the red solid curve) and the partial cross sections for the reactions used at the energies below 3 GeV. The sum of all these partial cross sections (the green dotted curve) matches the total cross section very well, below 2 GeV. At 3 GeV the sum is about 30% smaller than the total cross section. For the simulation, all the partial cross sections were normalized to keep their sum equal to the total cross section.

#	Process	Experimental data		Simulation		Comment
		Range, GeV	$d^n\sigma/dp^n$	Rate	$d^n\sigma/dp^n$	
1	$p\pi^\circ$	0.15 - 2.00	$\frac{d\sigma}{d(\cos\theta_{CM})}$	SAID	SAID	
2	$n\pi^+$	0.15 - 2.00	$\frac{d\sigma}{d(\cos\theta_{CM})}$	SAID	SAID	
3	$p\pi^+\pi^-$	0.40 -12.00	$d\sigma/dt$	total, used to extract (6)		
4	$p\rho^\circ$	1.00 - 2.50	$d\sigma/dt$	exp	exp	$\rho^\circ \to \pi^+\pi^- : \sin\theta_{CM}$
5	$\Delta^{++}\pi^-$	0.40 - 3.00	$d\sigma/dt$	exp	exp	$\Delta^{++} \to p\pi^+$
6	$p\pi^+\pi^-$	0.40 -12.00	$d\sigma/dt$	(3)-(4)-(5) non-resonant, by subtraction		
7	$p\pi^\circ\pi^\circ$	0.40 -0.80	$d\sigma/dt$	exp	phase space	
8	$n\pi^+\pi^\circ$	0.40 -0.80	$d\sigma/dt$	exp	phase space	
9	$p\eta$	0.70 -2.50	$\frac{d\sigma}{d(\cos\theta_{CM})}$	exp	exp	
10	$p\pi^+\pi^-\pi^\circ$	1.50 -10.00	$d\sigma/dt$	exp	phase space	
11	$n\pi^+\pi^+\pi^-$	1.50 -10.00	$d\sigma/dt$	exp	phase space	

Table 3: The reactions used to simulate the low energy background. The columns 4 and 6 show the source of the differential cross sections. Typically, the t-distributions have been measured. If the simulation was based on experimental data, the columns 5 and 6 indicate it with a note "exp". For the multi-meson states the uniform phase space distribution was used. The reaction (3) was not simulated, but used to extract the non-resonant contribution (6). The data were taken from the compilation [5] and from the HEPDATA reaction data base [6].

PYTHIA above 3 GeV and a compilation of the data on the dominant reactions below 3 GeV. These reactions are summarized in Table 3.

The total and the partial cross sections are presented in Fig. 2. The reaction admixture describes the total cross section very well below 2 GeV. At 3 GeV the sum is about 30% smaller than the total cross section. For the simulation, all the partial cross sections were normalized to keep their sum equal to the total cross section. Still, the discrepancy indicates that other processes, presumably with higher multiplicity step in between 2 and 3 GeV. This is demonstrated in Fig. 3.

The energy dependence of the π^+ multiplicity is relatively smooth, while the π^- and π° multiplicities have a dip just below 3 GeV. Because of this, about 6% of all simulated background events have π^- and π° multiplicities underestimated by $\sim$10%. The total event energy is not affected. We expect that this effect will not distort the estimate of the trigger rejection power by more than 1-2%.

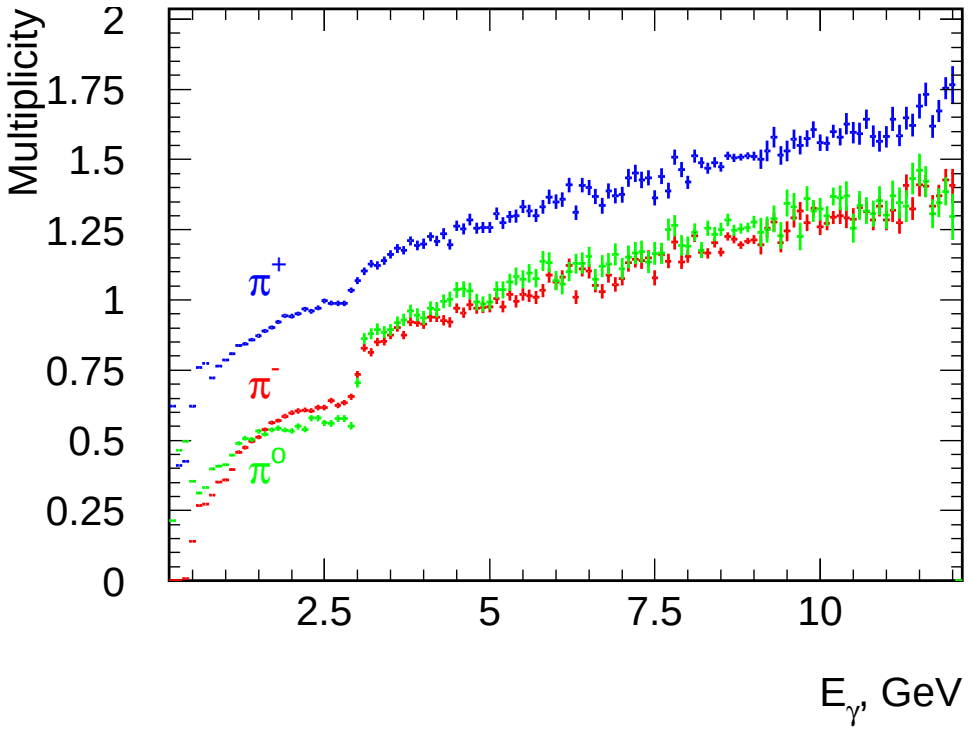

Figure 3: The average simulated multiplicities for pions. The dip at 2-3 GeV is an artefact of applying two different models for production below and above 3 GeV. Possible implications for the current studies are discussed in the text.

4 Trigger Simulation

The goal of the Level-1 trigger is to reduce the rate from electromagnetic and hadronic interactions seen by the GlueX detector to the level acceptable by the third level trigger, 200 kHz. In this section we investigate the feasibility of achieving this goal. In order to determine the trigger algorithm we perform a full GEANT [7] detector simulation. The reconstruction of energy deposition in the calorimeters is based on the realistic Monte Carlo (MC) simulation, i.e., the calibration coefficients used in the MC have been tuned according to the beam-test measurements [8]. We consider two sources of backgrounds:

- electromagnetic interactions of beam photons
- photoproduction of hadrons at low photon-beam energies, $E_\gamma \leq 8$ GeV

The electromagnetic background is modeled for Bremsstrahlung photons in the energy range of 1.1 MeV $\leq E_\gamma \leq$ 12.0 GeV[1]. The intensity of a photon beam is about 3×10^9. The electromagnetic interactions in this energy range originate mainly from a e^+e^- pair production and Compton scattering processes; the cross section of the later process dominates for $E_\gamma \leq 0.2$ GeV. The interaction rate of the beam photons in the target region constitute about 50 MHz and 140 MHz for the pair production and Compton scattering, respectively[2]. The polar angle and energy of $e^+(e^-)$ produced in $\gamma p \rightarrow e^+e^-$ reactions are shown in Fig. 4. The polar angle is defined as the angle between the beam direction and the momentum of $e^+(e^-)$. The corresponding distributions for γ and e^- originating from $\gamma e \rightarrow \gamma e$ processes are presented in Fig. 5. As can be seen from these plots, most e^+ (e^-) tracks produced from the gamma conversion go to the forward direction, i.e., they will be mainly seen by the 'forward' detectors, TOF and FCAL. At the same time, the low energy photons and electrons from Compton scattering are distributed over larger polar angles. The background rates of different detector components are listed in Table 4. The rate is calculated by counting the number of events with at least one hit in the corresponding subdetector.

	Start Counter	FCAL	BCAL	TOF
Rate (MHz)	2.5	5.9	0.4	41.9

Table 4: Subdetector rates for electromagnetic background. The thresholds to the hits definition in the FCAL and BCAL are set to 30 MeV.

Generation of hadronic interactions from photoproduction has been explained in Section 2. The hadronic background is defined as events produced at low beam energies,

[1]The low energy of photons is set close to the threshold of a e^+e^- pair production. For hadronic photoproduction the energy spectrum starts at $E_\gamma = 0.15\ GeV$, the production threshold of pπ

[2]Note, there is no vacuum beam pipe after the target. The interaction rates of beam photons in the entire detector range before the FCAL are 91 MHz for the pair production and 208 MHz for Compton scattering.

$E_\gamma < 8.0$ GeV. We study the trigger rate using hadronic events produced in the whole energy range of photons (0.15 GeV $\leq E_\gamma$) while a trigger probability is estimated for interactions of interest with events which beam energy satisfies $E_\gamma \geq 8.0$ GeV. Hereafter, we refer events with $E_\gamma \geq 8.0$ GeV to as hadronic 'signal' events. As has been discussed in Section 1, the topology of events generated with PYTHIA for a large photon-beam energy is somewhat similar to that predicted for exotic mesons. We also check the trigger efficiency by applying the trigger algorithm to signal MC samples generated for some 'typical' exotic decay channels, it will be discussed in Section 4.

To model hardware performance, we conservatively assume the electronics integration time interval of 100 ns for all subdetectors. In reality, this gate will be different for various detector components used in the trigger. The electronics pulse length for BCAL (100 ns) would presumably be the largest. We simulate multiple electromagnetic interactions in this time window by superimposing background beam photons on each event; on average about 300 beam photons pass the target region during 100 ns. The particles produced in the electromagnetic interactions are subsequently added to that from the standard generation mechanism.

In the next section we describe a simple trigger algorithm which is based on measurements of the number of hits in the start counter and energy deposition in the FCAL and BCAL.

4.1 Trigger Algorithm

To show the capabilities of the Level-1 trigger design, we develop a simple trigger algorithm which is able to provide sufficient background rejection and, at the same time, keep the trigger efficiency at the level close to 100%. The algorithm is based on conditional thresholds applied to a hit multiplicity in the start counter (SC) and energy depositions in the FCAL and BCAL. To determine these thresholds we study correlations among the number of hits in the SC and energies released in the calorimeters for background and signal events.

Hit multiplicities in the start counter for electromagnetic and hadronic backgrounds, and the signal events are shown in Fig. 6. As expected, a major fraction of electromagnetic background events, about 78.2%, produce no hits in the start counter. In contrary, almost all signal events (98.6%) have a track(s) within an acceptance of the start counter (the polar-angle acceptance lies between 3.0° and 134°) producing at least one hit. Note that in γp interactions there must be at least one charged track in the final state. The energy deposition in the FCAL and BCAL for signal and background events with no hits in the SC is presented in Fig. 7. The average energies deposited in the calorimeters are listed in Table 5. As can be seen from Fig. 7, the electromagnetic background releases relatively small energy in the BCAL. We reject electromagnetic and hadronic backgrounds requiring the BCAL energy in the event to be larger than 0.2 GeV and the total energy in the BCAL and FCAL to be greater than 2 GeV. We also apply a threshold on the FCAL energy $E_{\rm FCAL} > 30$ MeV. After these requirements, the rate for electromagnetic(hadronic) background is significantly reduced from 7.82 MHz (12 kHz)

to 4 kHz (0.2 kHz). The efficiency of hadronic 'signal' events with no hits in the SC is about 39%

It is worth mentioning that for most reconstructed exotic meson decays which produce no hits in the start counter, we would expect a relatively large energy deposition in the calorimeters. The thresholds on the energy deposition have to be further optimized using MC simulation for particular exotic decay channels. At the moment we assume that the contribution to the trigger rate from electromagnetic background with no hits in the start counter is negligible.

Process type	$E_{\rm BCAL}$ GeV		$E_{\rm FCAL}$ GeV	
	$N_{\rm SC}=0$	$N_{\rm SC}>0$	$N_{\rm SC}=0$	$N_{\rm SC}>0$
Electromagnetic	0.014	0.105	0.124	0.199
Hadronic $E_\gamma < 8$ GeV	0.277	0.578	0.212	0.304
Hadronic $E_\gamma > 8$ GeV	1.168	1.978	2.451	2.074

Table 5: Average energy deposition in the BCAL and FCAL for backgrounds and hadronic events with the beam-photon energy $E_\gamma > 8$ GeV. Energies are calculated for events with no hits ($N_{\rm SC} = 0$) and with at least one hit ($N_{\rm SC} > 0$) in the start counter.

Much larger contributions to the trigger rate come from events which have hits in the start counter. The energy distribution in the FCAL and BCAL for signal and background events with at least one hit in the SC is shown in Fig. 8. The electromagnetic and hadronic backgrounds can be substantially reduced by applying an asymmetric threshold on the energy deposition in both calorimeters, i.e. we reject low-energy events requiring $E_{\rm BCAL} + E_{\rm FCAL} \times 0.5/2.0 \geq 2.0$. This requirement is shown as a solid diagonal curve in Fig. 8. The resulting trigger rates and probabilities of accepting hadronic events with $E_\gamma > 8$ GeV for various thresholds are listed in Table 2. As can be seen, the total electromagnetic and hadronic rate does not exceed 150 KHz which is below our trigger requirements of 200 KHz. The probability of accepting hadronic events with $E_\gamma > 8.0$ GeV is about 93%. The energy spectra of beam photons for all hadronic interactions and those accepted by the Level-1 trigger are presented in Fig. 9.

We check the Level-1 trigger rate by applying the thresholds used for events with $N_{\rm SC} > 0$ to events which have no hits in the start counter. This implies that the start counter information is no longer used in the Level-1 trigger. We found that a trigger rate increases by only about 21 kHz due to the contribution from electromagnetic background, resulting to an overall trigger rate of ~ 170 kHz, which is still below 200 kHz.

In the next section we estimate the trigger efficiency using MC samples generated for some 'typical' exotic decays. In Section 3 we will discuss possibilities for the further improvement of the trigger algorithm.

4.2 FLT efficiency

4.3 Event Size

4.4 Outlook

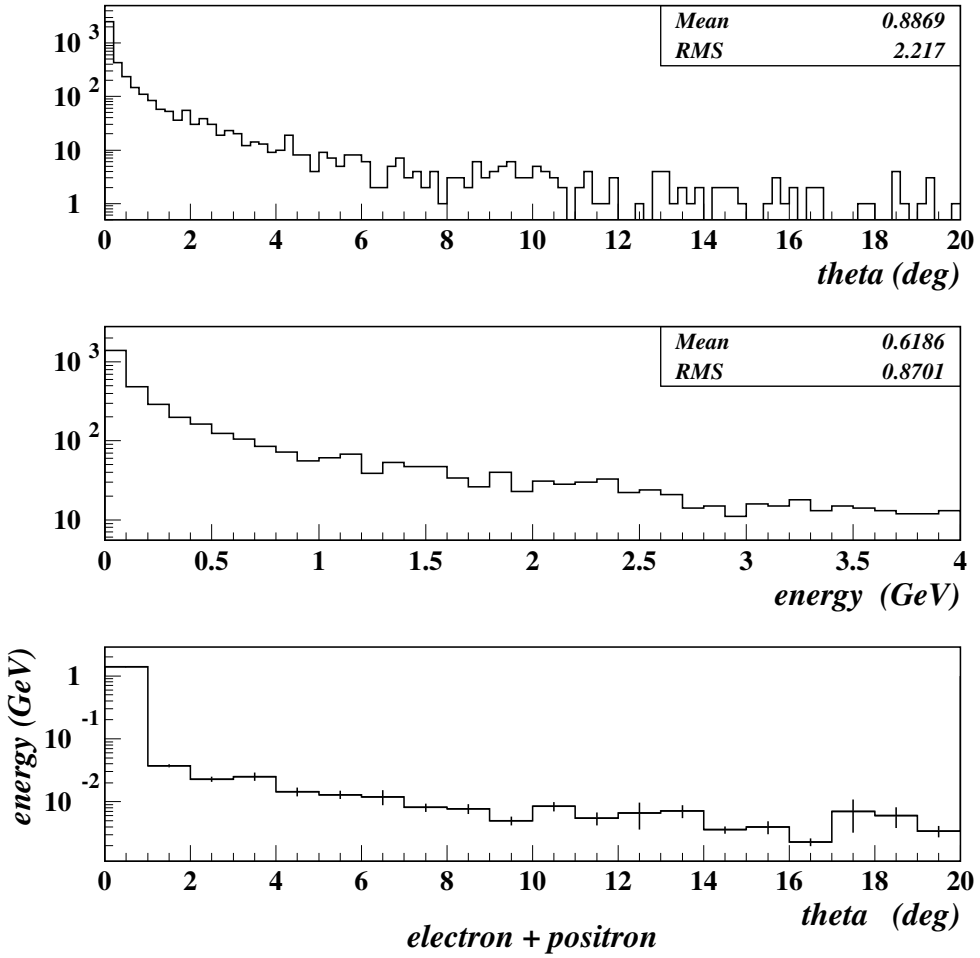

Figure 4: The polar angle (top), energy (middle), and energy versus polar angle (bottom) distributions for e^+ and e^- produced in $\gamma p \to e^+e^-$ interactions on target.

Trigger Rate (kHz)

	No cuts	$E_{\mathrm{FCAL}} > 30$ MeV	$E_{\mathrm{BCAL}} > 30$ MeV	$E_{\mathrm{FCAL+BCAL}}$
Electromagnetic	2180	317	214	60.5 (4.00)
Hadronic $E_\gamma < 8.0$ GeV	314.2	268.5	164.9	54.6 (0.23)
Hadronic $E_\gamma > 8.0$ GeV	32.7	30.9	30.8	30.2 (0.17)
Total				145.3 (149.7)

Trigger Probability (%)

Hadronic $E_\gamma > 8.0$ GeV	100.0	94.5	94.1	92.4

Table 6: The trigger rates and probabilities of accepting hadronic 'signal' events calculated for various thresholds sequentially applied to the energy depositions in the FCAL and BCAL. $E_{\mathrm{FCAL+BCAL}}$ denotes the energy-dependent threshold described in the text. The numbers in parentheses denote the additional contributions to the rate from events which have no hits in the start counter.

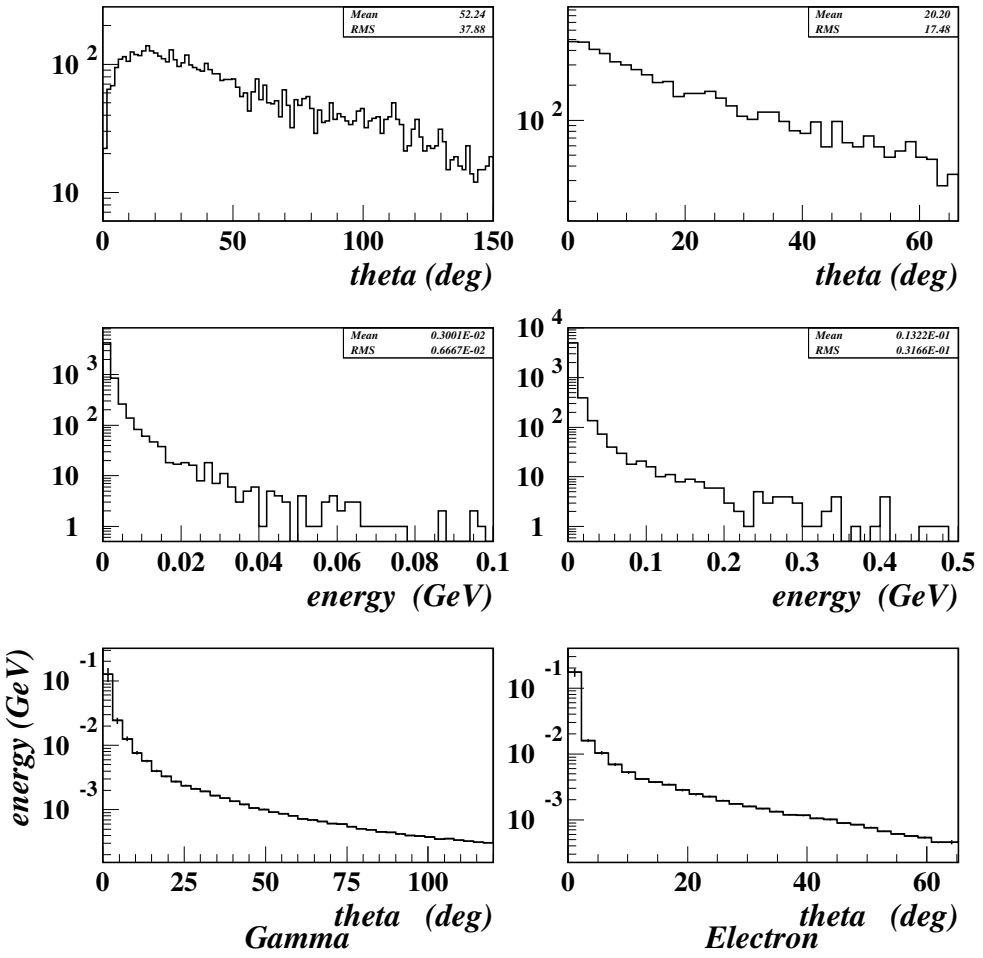

Figure 5: The polar angle (top), energy (middle), and energy versus polar angle (bottom) of photons (left column) and electrons (right column) for Compton scattering of the beam photons on target.

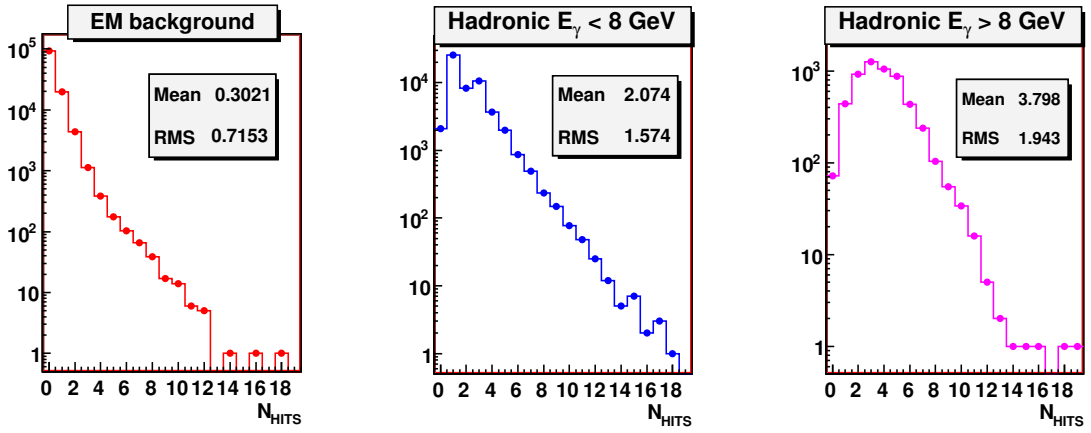

Figure 6: The hit multiplicities in the start counter for electromagnetic background (left), hadronic background (middle), and hadronic event with the beam energy in the signal region (right).

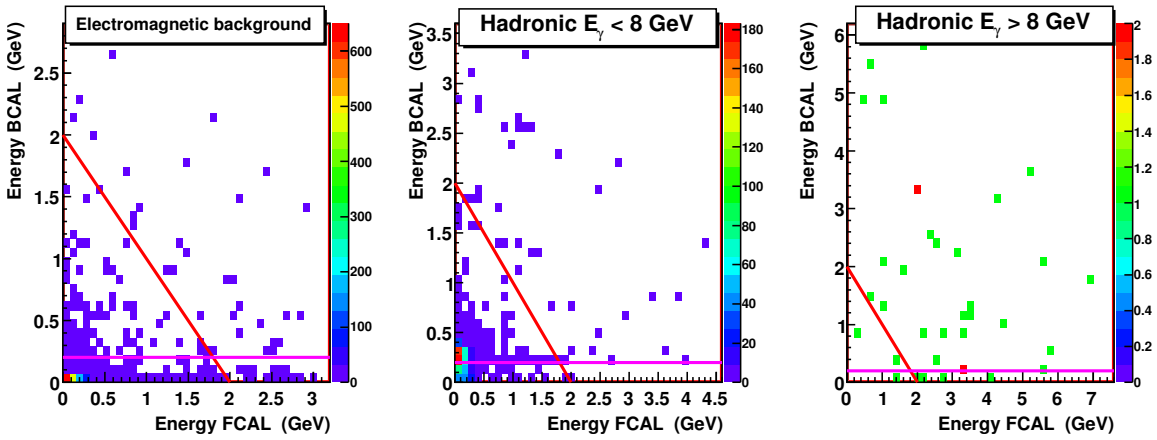

Figure 7: BCAL energy versus FCAL energy for events with no hits in the start counter for electromagnetic background (left), hadronic background (middle), and signal events (right). The solid curve represents the threshold applied in the analysis.

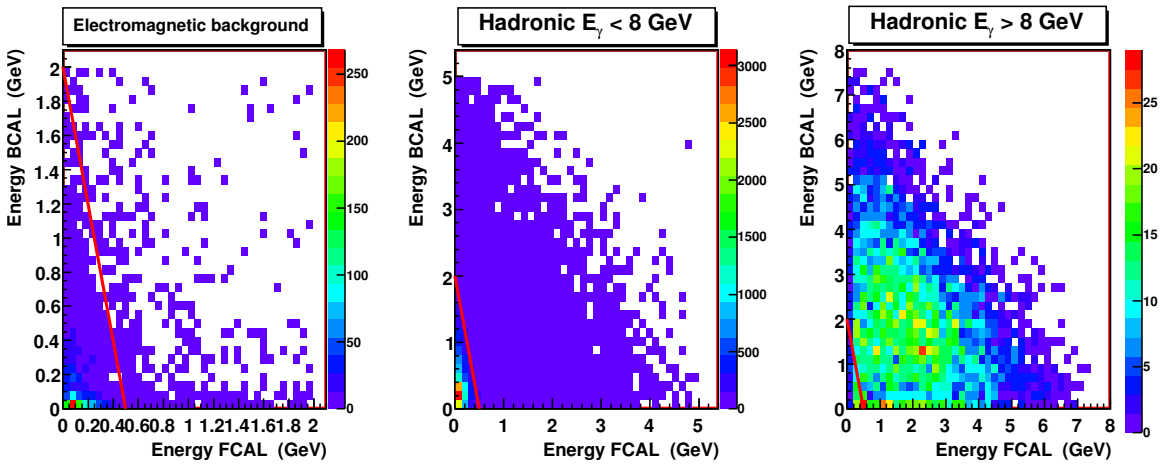

Figure 8: BCAL energy versus FCAL energy for events with at least one hit in the start counter for electromagnetic background (left), hadronic background (middle), and signal events (right). The solid curve represents the threshold applied in the analysis.

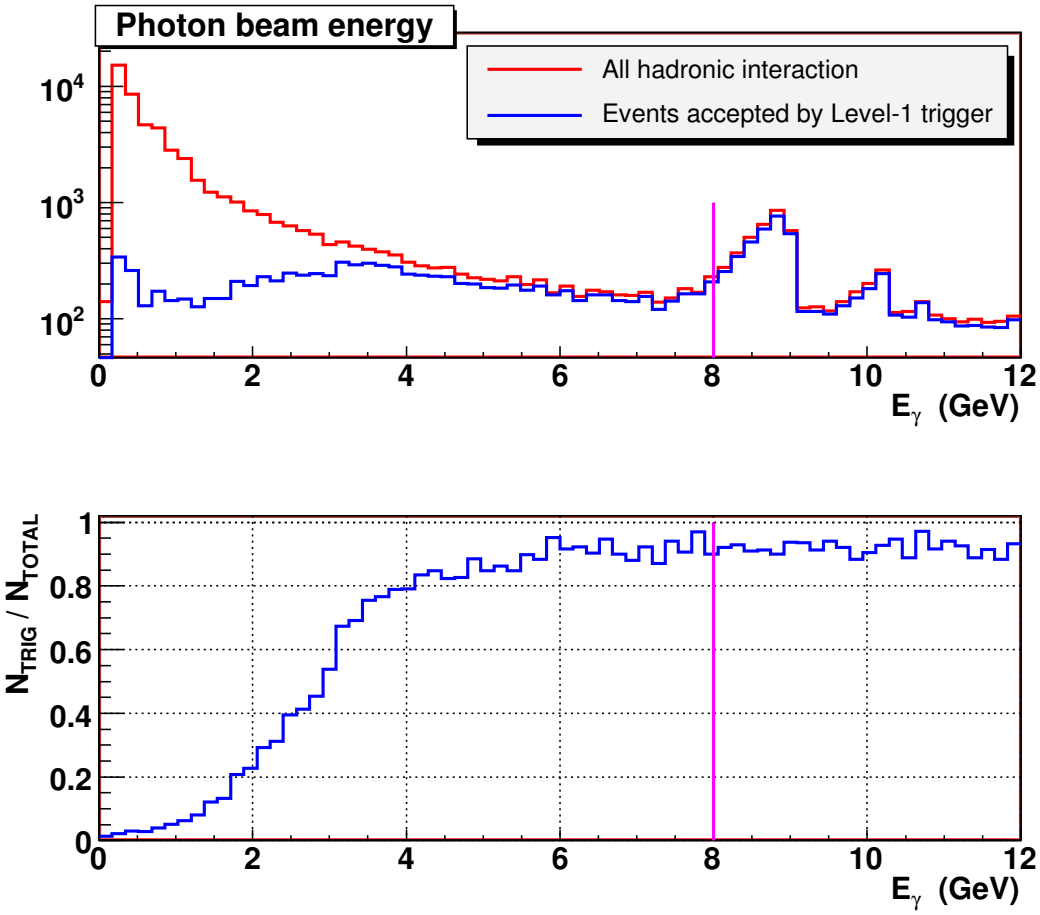

Figure 9: Energy spectra of beam photons for all events produced in hadronic interactions and those accepted by the Level-1 trigger (top). The trigger acceptance as function of the beam energy (bottom).

5 Conclusion

Add the contents

References

[1] A. Biselli et al. A search for QCD exotics using a beam of photons, 2002. Proposal.

[2] W. M. Yao et al. Review of particle physics. *J. Phys.*, G33:1–1232, 2006.

[3] Torbjorn Sjostrand, Leif Lonnblad, and Stephen Mrenna. PYTHIA 6.2: Physics and manual. 2001.

[4] S. S. Kamalov et al. Dispersion relation analysis of neutral pion photo- and electroproduction at threshold using the MAID and SAID solutions. *Phys. Rev.*, C66:065206, 2002.

[5] A. Baldini, V. Flaminio, W. G. Moorhead, Douglas R. O. Morrison, and (Ed.) Schopper, H. Total cross-sections for reactions of high-energy particles. Berlin, Germany: Springer (1988) 409 p. (Landolt-Boernstein. new series, 1/12B).

[6] HEPDATA: Reaction Database. URL http://www.slac.stanford.edu/spires/hepdata/.

[7] R. Brun et al. GEANT Detector Description and Simulation Tool, CERN Program Library (1993). We use GEANT version 3.21.

[8] GlueX collaboration. GlueX/Hall D Calorimeter Final Design and Safety Review. February 19-20,2008.